SANDWICH FILMS WITH GRAPHENE OXIDE NANOCORES

S. Rao*, J. Upadhyay, D. Liu, R. Das, D. Bhattacharyya

Centre for Advanced Composite Materials, Department of Mechanical Engineering. The University of Auckland, Auckland Mail Centre 1142, New Zealand
**s.rao@auckland.ac.nz*

Keywords: Nanocomposites, Sandwich films, Graphene Oxide, Gas Barrier.

Abstract

Single polymer composite films with PMMA facings and PMMA or PMMA-Graphene Oxide (GO) electrospun nano-fibre mat core were manufactured with an intention of application in various facets of engineering. Design of experiments based on mixture analysis was used to identify the solution concentration for obtaining uniform fibre diameters and their distribution throughout the electrospun core. The oxygen gas transmission rate (O_2GTR) and the permeance of the film (PO_2) were tested in OX-TRAN® Model 2/10, per standard ASTM F 2622 and modelled using series and parallel configuration. The sandwich films were manufactured using vacuum assisted compression moulding by laying the electrospun core between two thin layers of PMMA films. The analysis shows that 23% PMMA and 2% GO concentrations in the solution give approximately uniform fibre diameters and dispersion throughout the mat. The experimental results from the oxygen barrier tests revealed oxygen permeability values in the negative range for the sandwich films compared to 2.59 cc-mm/m^2 day for the neat PMMA films. The theoretically calculated values of permeation through the sandwich films were found to be in range of 0- 0.0224 cc-mm/m^{2}day The presence of GO, as low as 1%, in the nanofibre mat enhanced the oxygen barrier of the sandwich films by more than 100%.

1 Introduction

In the current age, polymer nanocomposites have gained importance because the properties of polymer matrices can be easily enhanced by appropriately incorporating relatively low volumes of nanofillers. Moreover, depending on the geometry of fillers, the relative properties of the resulting composites can be altered to meet the required performance. For example, 1D nanowires or 2D layered materials can be used to provide reinforcement to the matrix, improving functional properties, such as electrical and thermal properties [1]. Nanofillers such as graphite nanoplatelets [2], carbon nanotubes (CNTs) [3], graphene oxide (GO) [4] and functionalised graphene [5] have been extensively used due to their intrinsic mechanical and electrical conductivity properties.

In this study, GO has been used to enhance the gas barrier properties of the polymer matrix. Composite films of Poly-methyl methacrylate (PMMA) and composite nanofibres with GO fillers have been produced using the electrospinning technique. As the properties of the fibre mat depends on the fibre diameter and dispersion, statistical design of experiments based on mixture analysis has been used to identify the solution concentration for obtaining uniform fibre diameters and their distribution throughout the electrospun core. Sandwich films were

manufactured by sandwiching the electrospun core between PMMA facings using vacuum assisted compression moulding, with the idea of using them as gas barriers or filters. The objective was achieved as the experimentally obtained oxygen permeability values for the sandwich films were in negative range compared to 2.59 cc-mm/m^2 day for the neat PMMA film, thus displaying significant enhancement in the oxygen barrier property.
Oxygen permeation through electrospun nanofibre core was studied using conduction based model for flow through non-woven mats considering the geometric aspects of the porous media. To analyse the effect of GO fillers present in the PMMA nanofibres, permeability models for polymer matrices with sheet like fillers were adopted to predict the permeability of the sandwich films prepared for this study. The standard unit for permeability is barrer and 1 barrer is defined as $10x10^{-10}$ cc (STP).cm/cm^2.s.cm Hg. In this work, permeability results are presented in the unit cc –mm /m^2 day.

1.1 Gas barrier modelling:

1.1.1 Permeability of gases through homogeneous films

Permeability of a film represents the amount of fluid passing through the film material of a certain cross-sectional area and thickness in a specified amount of time. It involves two mechanisms: thermodynamic solubility of the permeant on the surface of the films and kinetic diffusion of the permeating molecules across the film to the other surface [6-9]. The solubility of a gas entering a polymer matrix is determined by the enthalpy change and the free volume available in the matrix. The ideal sorption process is governed by the Henry's law. The diffusion of permeating molecules through the film depends on the free volume available between polymer chains, termed as Fickian diffusion, and obeys Fick's first and second laws [6]. In general, the permeability of a homogenous media can be obtained using Darcy's law of diffusion for viscous flow [10] as given below:

$$k = \frac{\mu Q d}{A \Delta p} \tag{1}$$

where, k is the Permeability constant, μ is the viscosity of the gas, Q is the flow rate of the gas, d is the thickness of the test specimen, A is the area of the test specimen and Δp is the pressure difference across the test specimen.

1.1.2 Permeability of gases through nonwoven fibrous mats

Fibrous mats are extensively used in applications, such as advanced air and liquid filtration, catalysis and gas sensors due to their large surface area-to-volume ratio at relatively lower weights. The gas flow through fibrous mats differs from the homogeneous systems in regards to their porosity and the nature of the media (fibrous). The larger surface area of fibres offers strong resistance to fluid motion, which in effect is driven primarily by the viscosity of the fluid. As the fibre diameter approaches to a size of nanometer scale, the mean free path of gas molecules becomes comparable to the fibre diameter [11]. Hence, aerodynamic slip at the fibre surface may arise, making the linear relationships between flow rate and pressure drop that is apparent in laminar flows, less applicable [12-15]. Therefore, to analyse the gas flow through fibrous mats, a thermodynamic flow regime in the specimen must be established, which is possible by determining the Knudson number (Kn), related to different flow regimes [12, 15]:

a) Continuum flow regime; Kn $<10^{-3}$
b) Slip flow regime; $10^{-3}<$ Kn <0.25
c) Transition flow regime; $0.25 <$ Kn <10
d) Free molecule regime; Kn >10

Once the flow regime has been identified, the permeability of the films can be calculated

using appropriate relationships. For example, the conduction based model modified by Tomadakis and co-workers [13] that predicts the permeability of a fibrous media to some accuracy, taking into account the bulk diffusion tortuosity, is expressed as,

$$\frac{k}{r^2} = \frac{\varepsilon}{8\,(\ln \varepsilon)^2}\,\frac{(\varepsilon - \varepsilon_p)^{\alpha+2}}{(1-\varepsilon_p)^{\alpha}\,[(\alpha+1)\varepsilon - \varepsilon_p]^2} \tag{2}$$

where, k is the permeability constant, r is the fibre radius, ε is the porosity of the structure, ε_p is the percolation threshold for porosity and α is the constant of bulk tortuosity.

1.1.3 Permeability of gases through polymer nanocomposites with sheet like fillers

There are several models used to predict permeability of polymer nanocomposites with thin sheet-like fillers. By enlarge, the model predictions fall within the range given by series and parallel models, that take into account mainly the permeability and volume fraction of the polymer matrix and the fillers, [6] as described below:

Series model that defines the upper bound considering orientation of fillers across the direction of permeation:

$$P_{nc} = \frac{P_p P_g}{\phi_p P_g + \phi_g P_p} \tag{3}$$

and, Parallel model that defines the lower bound considering orientation of fillers parallel to the direction of permeation:

$$P_{nc} = \phi_p P_p + \phi_g P_g \tag{4}$$

where P denotes permeability, ϕ is the volume fraction and the subscripts p and g represent the matrix and GO filler respectively.

However, the permeability of composite films with sheet like fillers also depends on the geometric parameters of the filler and their orientation in the film with respect to the gas flow direction, in essence decreasing the permeability of the system. Therefore, to account for the orientation and aspect ratio of the fillers, a '*tortuosity factor*' (τ) is derived which is the ratio of the actual distance (d') the permeant is forced to travel to the minimum distance of travel possible (d) that it would have traveled in the absence of the filler and is expressed in terms of the length (L), width (W), and volume fraction of the sheets (ϕ) [14], as follows:

$$\tau = \frac{d'}{d} = 1 + \frac{L_g}{2W_g}\,\phi_g \tag{5}$$

The effect of tortuosity on the permeability is expressed as

$$\frac{P_{nc}}{P_p} = \frac{1-\phi_g}{\tau} \tag{6}$$

where P_{nc} and P_p represent the premeabilities of the polymer nanocomposite and pure polymer, respectively.

Permeation through nanocomposite films is minimum when all the nano-filler sheets are aligned across the traveling path of the fluid. However, in practice, the fillers can be oriented at different angles to the flow as depicted in fig. 1, resulting in a lower effective aspect ratio. To account for the effect of filler orientation on overall tortuosity, an order parameter S [14] is defined as follows: where θ is the angle between the direction of the gas flow (**n**) and the GO sheet normal (**p**) unit vectors as shown in Fig.1. The order parameter can range from 1 ($\theta = 0$), indicating planar orientation of the filler across the path of permeating gas to -1/2 ($\theta = \pi/2$) indicating perpendicular or orthogonal orientation, and a value of 0, for random orientation of

the sheets.

$$S = \frac{1}{2}\langle 3cos^2\theta - 1\rangle \tag{7}$$

The angular brackets denote averaging over all the sheets in the system. The tortuosity factor as expressed by Eq. 5 can be modified to include the orientation order of the fillers, and using Eq. 6, the nanocomposite permeability is given by

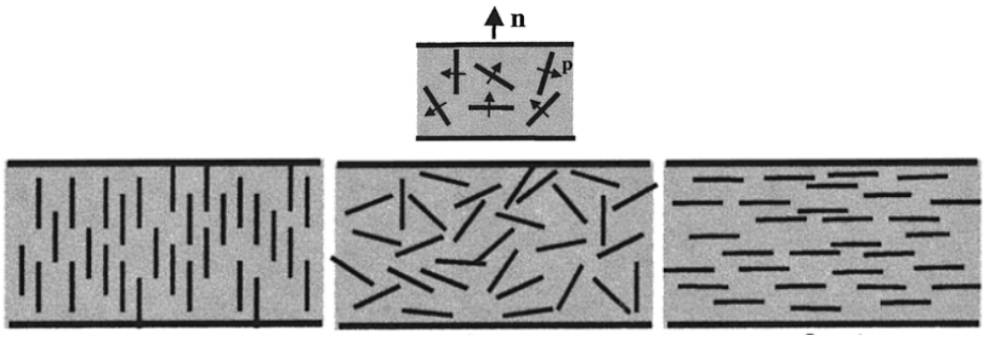

S = -1/2 S = 0 S = 1

Fig.1 Filler orientation with respect to the gas flow direction

$$P_{nc} = \frac{(1-\phi_g)P_p}{1+\frac{L}{2W}\phi_g\left(\frac{2}{3}\right)(S+\frac{1}{2})} \tag{8}$$

In case of multi layered systems, a series resistance model can be used to predict permeability of the system [15], using the following expression.

$$\frac{t_f}{P_f} = \frac{t_1}{P_1} + \frac{t_2}{P_2} + \frac{t_3}{P_3} \tag{9}$$

where P_f is the effective permeability of the three-layered sandwich film, t_f is the total thickness of the three-layered sandwich film and 1,2 and 3 are the number of layers.

2 Materials, manufacturing and testing

Graphene oxide (GO) was synthesized from Graphite flakes (bought from Sigma-Aldrich) using modified Hummer's method [6]. The other primary materials used in this study are N-dimethylformamide (DMF, Anhydrous, 99.8%) purchased from Sigma-Aldrich, tetrahydrofuran (THF) bought from ECP Ltd (Romil, UK), and PMMA..

Graphene oxide, which was in the form of films was ground to fine particles (325 mesh) using a centrifugal shear mixer so that it could be well dispersed in the solvent. A weight ratio of the solvent mix (DMF:THF), maintained to 2:1 and was mixed for 15 min in a sonication bath. Varying amounts of GO was added to the solvent solution and the sonication was continued for another 15 min, after which the solution was stirred at room temperature for 8 hours and mixed in the sonication bath for 15 minutes. PMMA was weighed, and transferred to the beaker containing the GO-solvent solution mixture which was stirred using magnetic stirrers for 5 hours. A syringe and needle was used for electrospinning, and an aluminium foil was used as a stationary target. A heater and a dehumidifier were used to control the temperature and humidity in the test chamber, respectively. A humidity level of 50-60%, a temperature range of 15-20°C, a flow rate of 2 ml/h, voltage of 20 kV, and a spinning distance of 100 mm were maintained. The synthesized GO material was characterised using FTIR, and the fibre diameters were measured using SEM images of electrospun mats obtained from different solution concentrations in an image analysis tool (UTHCSA) environment. The oxygen gas transmission rate (O_2GTR) and the permeance of the film (PO_2) were tested in OX-TRAN®

Model 2/10, per standard ASTM F 2622.

3 Results and discussion

3.1 Mixture analysis

Statistical design of experiments based on mixture analysis was used to identify the solution concentration for obtaining uniform fibre diameters and their distribution throughout the electrospun core. This revealed possible uniformity in fibre diameters and dispersion when the concentrations of PMMA and GO in the solution were 23% and 2%, respectively [4]. Vacuum assisted compression moulding at a pressure ~0.5 bar and a temperature of 160°C was adequate to form sandwich films without crushing the electrospun core.

3.1.1 Fibre distribution

Mixture analysis can be useful in determining the optimum proportions of the PMMA and GO required for the desired fibre dispersion in the mat. The global simplex domain for three component systems is shown in Fig. 2, where the vertices denote the pure components and components A, B and C represent PMMA, DMF+THF(2:1) and GO, respectively.

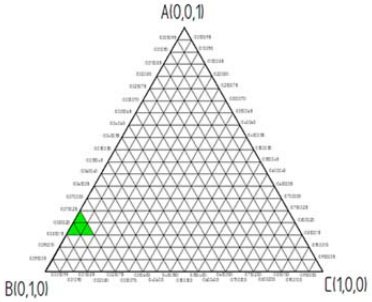

Fig. 2 Simplex lattice space for 3 components

However, it may not be practically possible to have nanofibres of all the pure components using electrospinning. Therefore, the analysis has to be confined to a region in the global simplex domain. This can be established experimentally by testing different solutions under different conditions. The green (shaded) region in Fig.2 shows the simplex space for this particular solution and filler type. The concentrations were varied for PMMA from 0.25-0.35, for DMF+THF from 0.75-0.8 and for GO from 0.0-0.1. It was observed that the nanofibres in this range were bead free. Two degrees and three components (3,2) were considered, which resulted in six data points. The coefficients were determined using Matlab environment by solving the six simultaneous equations resulting from the six data points. To obtain the fibre distribution in an area, the mats were graded from 0-10. Accordingly, a full (100%) coverage of a given surface area by nanofibres corresponded to grade 10, and no fibres in a selected surface meant grade 0. The percentage dispersion corresponding to their relevant grading is listed in Table 1, and the contour plot of the dispersions over the simplex space is shown in Fig. 3.

A	B	C	Level
0.1980	0.80	0.0020	6.3
0.1960	0.80	0.0040	7.5
0.1900	0.80	0.0100	7.3
0.2156	0.78	0.0044	8.0
0.2277	0.77	0.0023	7.0
0.2254	0.77	0.0046	8.8

Table. 1 different concentration

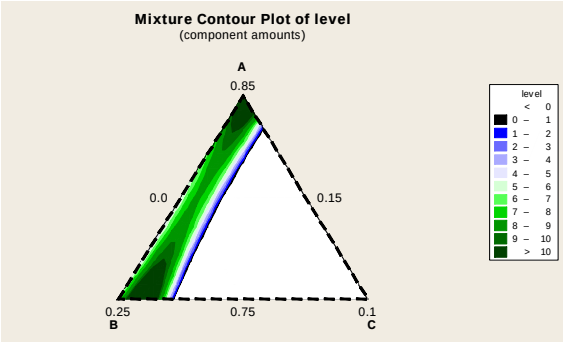

Fig.3 Contour Plot of levels after mixture analysis

3.1.2 Fibre diameters

The fibre diameters were measured using SEM images of electrospun mats obtained from different solution concentrations in an image analysis tool (UTHCSA) environment. The average diameter obtained at ten different locations on the fibre was used, and the results are listed in Table 2. The fibre diameter increases with an increase in the concentration of PMMA-GO, because of the increase in viscosity of the solution, which in turn reduces the stretching of the fibres during electrospinning resulting in thicker fibres. However, the uniformity of the fibre diameters in the mat was obtained with the solution concentration of PMMA 23% and 2% GO.

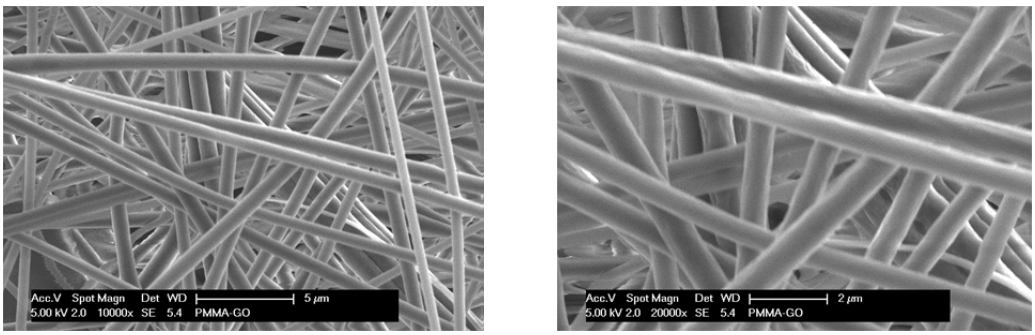

Fig. 4 SEM images of nanofibres at 23% PMMA and 2% GO

PMMA-GO Concentration	18-2	20-1	20-2	20-5	22-2	23-1	23-2
Average diameter (nm)	330	419	457	407	484	750	671
% dispersion	80	70	75	73	67.15	70	88

Table. 2 Average diameter and percentage dispersion of PMMA/GO nanofibres at different concentrations

3.2 Gas barrier modelling

3.2.1 Conduction model for nanofibre mats

Three cases of filler loading were considered for experimental tests, viz: no filler loading, 1% GO loading, and 2% GO loading. The Knudsen number values for oxygen permeating through PMMA nanofibre mat corresponding to the average fibre diameter for the tested samples lie between 6.39-14.54 indicating the flow regimes to be predominantly transition and free molecule, i.e. a no slip condition occurs at the fibre surface. Hence, the oxygen flow through our samples can be characterised by models where the flow is viscous and laminar with no slip boundary condition. The permeability constant values for the PMMA facings and nanofibre mat were obtained using Eqs.1 and 2, respectively. The values for percolation threshold for porosity ε_p and bulk tortuosity constant α for 3D flow through randomly oriented

fibrous structure for Eq. 2 were taken as 0.037 and 0.965 [16], respectively.

GO loading (%)	Porosity	Theoretical permeation value through the sandwich film (cc-mm / m^2 – day)	Experimental permeation through the sandwich film (cc-mm / m^2 – day)
0	0.3	0.0438	0.0448
1	0.30	0.0224	-28.76
2	0.33	0.0184	-10.08

Table. 3 Theoretical and experimental values of permeation for sandwich films considering the analytical models for permeation through non-woven nano-fibre mats

The permeability constant of sandwich films was obtained using Eq. 9, considering the PMMA and nonofibre mat to be in a parallel arrangement. Using the known permeability constant for the sandwich film, the permeation of oxygen through the sandwich film was then obtained by using Eq. 1. The permeation values listed in Table 3 indicates that the predicted permeation values of the samples with no GO loading correlate well, but the model slightly over predicts the permeation of oxygen through sandwich films with GO fillers in them. It has to be noted that the negative values indicate that the films are impermeable. The discrepancy in the correlation may be due to the presence of the fillers within the nanofibre core and/or their orientation to the gas flow that have not been accounted for in the conduction model.

3.2.2 Models accounting for the fillers content in the nanofibre core

Models that account for the filler content in the polymer are expressed in Eqs.3 and 4, providing the upper and lower bounds by considering the volume fraction of the filler within the polymer and the unidirectional arrangment of these fillers with respect to the gas flow. The permeation values of the sandwich films were obtained in a similar way as discussed in section 3.2.1, but here Eqs. 2 and 3 were used to calculate the permeation values of the nanofibre core. The permeation values of the sandwich films are listed in Table 4.

GO loading (%)	Porosity	Theoretical permeation value through the sandwich film (cc-mm / m^2 – day)		Experimental permeation through the sandwich film (cc-mm / m^2 – day)
		Series	Parallel	
1	0.30	0.00	0.0034	-28.76
2	0.33	0.00	0.0037	-10.08

Table. 4 Theoretical and experimental values of permeation for sandwich films considering upper and lower bound analytical models for permeation through polymer composites with sheet-like fillers

Only the volume fraction of the filler has been accounted for in Table 4, but the other factors, such as packing factor and orientation of the fibres, were not included. However, the values predicted by these models mark the upper and lower bounds for permeation and the predictions from most models will fall between these bounds. The permeability values predicted by using series model are zero as the perfect arrangement of impermeable GO fillers across the permeant path will completely obstruct the fluid flow.

3.3 Gas barrier modelling: Models accounting for the orientation of fillers in the nanofibre core

Orientation of fillers in directions other than perpendicular to the fluid flow reduces the effect of aspect ratio significantly, especially in the case of short fillers. When the filler sheets are aligned perfectly parallel to the direction of permeation, the permeability of the system nearly approaches to that of a monolithic polymer. Therefore, the orientation factor was calculated using Eq. 7, and the permeability of the nanofibre core was obtained using Eq. 8. The permeability of the sandwich film was obtained using Eq. 9. These permeability values are listed in Table 5 for the three cases where the orientation of the fillers vary from $\theta = 0\text{-}\pi/2$ and hence, order parameter S varying from 0-1.

In Table 5, the predicted permeation values are much higher compared to those of the experimental ones. However, the high values of permeability may be due to a combination of the GO filler arrangement, fibrous nature of the mat and porosity between the overlapping fibres.

GO loading (%)	Porosity	Theoretical permeation value through the sandwich film (cc-mm / m^2 – day)			Experimental permeation through the sandwich film (cc-mm / m^2 – day)
		S = 1	S = 0.5	S = -0.5	
1	0.30	0.001649	0.001996	0.003449	-28.76
2	0.33	0.001139	0.001479	0.003675	-10.08

Table. 5 Theoretical and experimental values of permeation for sandwich films considering tortuosity based analytical models for composites with sheet-like fillers

4 Summary

Composite nanofibre mats with GO fillers and PMMA matrix were produced using the electrospinning technique to improve the functionalities and mechanical properties of the film. The solution concentration for obtaining uniform fibre diameters and their distribution throughout the electrospun core was determined via mixture analysis using statistical design of experiments. The corresponding PMMA and GO concentrations were 23% and 2%, respectively. Vacuum assisted compression moulding at pressure of 1 bar and temperature of 160°C was adequate to form sandwich films without crushing the electrospun core. The oxygen gas transmission rate (O_2GTR) and the permeance of the film (PO_2) were tested in *OX-TRAN*® Model 2/10, according to standard ASTM F 2622 and modelled using series and parallel configurations. The barrier property of the sandwich films with PMMA facings and PMMA-GO nanofiber cores is found to be very good with significantly low experimentally obtained oxygen permeation values compared to neat PMMA films. A direct correlation between the permeation values and the filler loading could not be established, as the porosity of the mat and the dispersion of the fillers may not be uniform and the values used in modelling were mainly from SEM and TEM micrographs which concentrate on relatively small areas. This aspect will be further investigated in the future.

REFERENCES

[1] R. Sengupta, M. Bhattacharya, M. S. Bandyopadhyay and A. K. Bhowmick. A review on the mechanical and electrical properties of graphite and modified graphite reinforced polymer composites. Progress in Polymer Science. Vol 36 (2011), p 638-670

[2] K. Wakabayashi, C. Pierre, D. A. Dikin, R. S. Ruoff, T. Ramanathan L. C. Brinson, J. M. Torkelson, Polymer-graphite nanocomposites: Effective dispersion and major property enhancement via solid-state shear pulverization. Macromolecules. Vol. 41 (2008), p. 1905

[3] J. C. Grunlan, A. R. Mehrabi, M. V. Bannon, J. L. Bahr, Water-based single-walled-nanotube-filled polymer composite with an exceptionally low percolation threshold. Adv. Mater. Vol 16 (2004), p. 150

[4] Rao, S., D. Liu, P. Jaiswal, S. Ray, D. Bhattacharyya. Electrospun Nanofibre Cores Containing Graphene Oxide for Sandwich Films: Manufacturing and Analysis. Advanced Materials Research, 2011. 410-410: p. 26-30.

[5] J. L. Vickery, A. J. Patil, S. Mann, Fabrication of Graphene – Polymer Nanocomposites with Higher-order Three-Dimensional Architecture. Adv. Mater. Vol. 21 (2009), p.2180

[6] Shields, R.J., Characterisation of the Mechanical and Oxygen Barrier Properties of Microfibril Reinforced Composites. (2008).

[7] Gonzo, E.E., M.L. Parentis, and J.C. Gottifredi, Estimating models for predicting effective permeability of mixed matrix membranes. Journal of Membrane Science, Vol. 277, 1-2 (2006): p. 46-54.

[8] Robeson, L.M., ed. Gas Permeability in Polymer Blends. Polymer charactersiation techniques and their application to blends, ed. G.P. Simon, Oxford University Press. (2003) p. 288 - 312.

[9] Kamal, M.R. and I.A. Jinnah, Permeability of Oxygen and Water Vapor through Polyethylene / Polyamide Films. Polymer Engineering and Science, vol. 24 (1984), p. 17.

[10] Gibson, P., H. Schreuder-Gibson, and D. Rivin, Transport properties of porous membranes based on electrospun nanofibers. Colloids and Surfaces a-Physicochemical and Engineering Aspects, vol. 187 (2001), p. 469-481.
[11] Brown, R.C. and R.C. Brown, Air filtration: an integrated approach to the theory and applications of fibrous filters / R.C. Brown, Oxford ; New York : Pergamon Press, (1993).
[12] Hosseini, S.A. and H.V. Tafreshi, Modeling permeability of 3-D nanofiber media in slip flow regime. Chemical Engineering Science. Vol. 65(6) (2010): p. 2249-2254.
[13] Tomadakis, M.M., Viscous Permeability of Random Fiber Structures: Comparison of Electrical and Diffusional Estimates with Experimental and Analytical Results. Journal of Composite Materials. Vol. 39(2) (2004): p. 163-188.
[14] Bhardwaj, R.K., Modeling the Barrier Properties of Polymer-Layered Silicate Nanocomposites. Macromolecules, American Chemical Society. Vol. 34 (2001): p. 9189-9192.
[15] Nielsen, L.E., Models for the Permeability of Filled Polymer Systems. Journal of Macromolecular Science, (1967). Part A - Chemistry.
[16] Sambaer, W., M. Zatloukal, and D. Kimmer, 3D modeling of filtration process via polyurethane nanofiber based nonwoven filters prepared by electrospinning process. Chemical Engineering Science. 66(4) (2011): p. 613-623.